Investigating efflorescence in salt-cement composites: The impact of surface inclination and salt waste types on resource-efficient construction materials

Vesna Pungercar [a,b,*], Yee Wu [b], Clarimma Sessa [c], Thomas Kränkel [b]

[a] *Rudolfovo - Science and Technology Center Novo mesto, Slovenia*
[b] *Technical University of Munich, TUM School of Engineering and Design, Department of Materials Engineering, Center for Building Materials, Chair of Materials Science and Testing, Germany*
[c] *Technical University of Munich, TUM School of Engineering and Design, Chair of Conservation-Restoration, Art Technology and Conservation Science, Germany*

A R T I C L E   I N F O

A B S T R A C T

Disposing of excess salt from seawater desalination and the potash industry presents substantial ecological risks worldwide. This underscores the pressing need to explore reuse possibilities to mitigate environmental damage. One potential solution involves incorporating salt waste into building construction, especially in environments with low air humidity. However, this integration affects composite materials' mechanical and hydrothermal properties and results in efflorescence on the material surface. This study investigates how different surface inclinations and two types of salt waste affect efflorescence in salt cement mixtures. The primary goal of this research is to design more resource-efficient building materials by reducing cement usage while improving understanding of optimized surface design in indoor construction applications. Experimental in-situ measurements employing Confocal Laser Scanning Microscopy (CLSM) and Macro X-ray fluorescence scanning (MA-XRF) were conducted to examine salt crystallization accumulation on the salt cement surface. Our findings indicate higher efflorescence on concrete-salt surfaces with steeper inclinations (30–60 %). Furthermore, salt waste from the potash industry exhibits greater efflorescence than desalination salts, attributed to its higher sodium chloride content. This research contributes to a deeper understanding of the interactions among salt waste, cement, and surface characteristics, providing valuable insights for future advancements in construction materials science.

1. Introduction

Today, salts are abundant by-products in desalination plants and potash production processes [1]. Edward Jones et al. discovered that in 2018, with 15,906 operational desalination plants worldwide, the global volume of salt waste reached 8.45 million cubic meters per day, with nearly half originating from the Middle East and North Africa [2,3]. In 2022, there were already 22,000 desalination plants, expected to rise yearly by between 6 % and 12 % [3]. The most common ionic compound in salt waste from water desalination is sodium chloride (NaCl), about 77 wt%. The remaining salt components are $MgCl_2 \cdot 6\ H_2O$ (10 wt%), $MgSO_4 \cdot 7\ H_2O$ (6 wt%),

$CaSO_4\cdot2\ H_2O$ (3.9 wt%), and KCl (2 wt%) [4]. At the same time, in potash production, salt waste ranging from 0.05 to 0.43 million cubic meters is generated daily, primarily originating from Russia, Belarus, and Canada [5–9]. Together, approximately 8.88 million cubic meters of salt waste are generated globally every day, and it consists of NaCl (94.8 wt%), KCl (2.6 wt%), $MgCl_2\cdot6\ H_2O$ (0.8 wt%), $MgSO_4\cdot7\ H_2O$ (0.2 wt%) [10,11], and soil. Unfortunately, much of this waste is disposed of in the environment (see Fig. 1), contributing to heightened water salinity and temperature. These changes have detrimental effects on both flora and fauna, posing a severe threat to plant and aquatic life, particularly in areas of high concentration [1,12]. Using salt waste has the potential to mitigate salt contamination of the environment and reduce reliance on energy- or CO_2-intensive materials.

Incorporating salt into construction materials is an emerging concept with historical precedents. Ancient examples include the use of salt-rich mud mortar in Karshif bricks in Egypt [13,14] and seawater-mixed lime concrete by the Romans [15–18]. More recently, salt-based materials have been explored for nuclear waste containment in Germany [19]. Manufacturing methods for salt-based materials include compression [20–22], crystallization [23–25], and additive manufacturing [26–29]. One of the key motivations for salt-based materials is reducing reliance on cement, a major contributor to CO_2 emissions due to clinker manufacturing and raw material extraction [26–30]. Studies have examined cement mixtures with salt or seawater, finding initial strength increases followed by long-term deterioration due to chemical interactions [30–32].

Even though salt in a concrete mixture may diminish mechanical properties, it still demonstrates numerous positive attributes. It boasts antibacterial qualities, is inflammable, and assists in maintaining humidity and heat. Moreover, its crystallization can have advantageous and disadvantageous impacts on material properties. Gotti et al. suggest that adding salt to cement can significantly reduce water penetration depth, with crystallization playing a pivotal role in Roman hydraulic concrete. Also, certain types of sandstone form a salt crystallization barrier that helps prevent decay as it fills the pores and limits the further infiltration of substances [10,33]. However, that same research also suggests that building materials containing salts in coastal areas may weaken over time due to repeated dry-wet cycles [32,34]. Furthermore, beyond construction, salt's beneficial properties in therapies like speleotherapy [35–38] and halotherapy [39–42] suggest potential integration into building materials for enhanced human health benefits. An increase in salt crystallization on the material surface might result in a higher concentration of salt particles in the air. Breathing more salt particles in the air could clean the lungs, which is beneficial for respiratory health. However, further investigation is required into building surface and salt behavior [43,44].

Salt crystallization or efflorescence is a naturally occurring deterioration pattern with salts in building materials [45,46]. Understanding the mechanism of efflorescence is crucial for comprehending how salts can be incorporated with cement. Salt crystallizes when salt dissolved in water precipitates out of solution due to oversaturation, influenced by temperature and humidity [46,47]. For instance, in the case of sodium chloride salts, it is commonly known that they crystalize at room temperature (21°C) and have a relative humidity lower than 75 %. However, salts of different chemical components crystallize under various environmental conditions. Sodium sulfate's crystallization process differs with relative humidity lower than 50 % and higher than 50 % [33].

Salt solutions can crystallize on the surface or within pores in cement-based materials. Gomez et al. studied how volume, surface free energies, and local curvature affect nucleation [47,48]. They found that surface geometry changes nuclei's critical size and path to equilibrium. Surface curvature significantly affects crystallization onset and initial crystal size. On curved surfaces, critical crystal size can deviate from that on low inclination surfaces [49]. Similarly, Amanda J. Page and Richard P. Sear's research [50] on noble gases and methane crystallization found specific crystal alignment in wedges. Using Monte Carlo simulations, they showed nucleation rates increase with surface inclination from 0° to 55°, then decrease at higher angles [50].

Surface inclination affects not only nucleation size and rate but also salt accumulation. Nachshon et al. showed that the surface angle influences capillary water distribution during evaporation, creating different pressure levels and speeds [51]. Higher inclinations lead to more salt accumulation at higher positions due to changes in solute transport. Capillary-driven flow enhances salt crystal growth by forming conduits on non-porous surfaces, allowing electrolytes to wick upwards. This crystal growth continues through capillary flow and water evaporation. Relative humidity and flow dynamics also impact salt deposition patterns. Upward capillary flows from evaporation can overpower downward sedimentation, pushing particles to higher areas and increasing salt accumulation [51,52]. With lower humidity, evaporation is faster and occurs within salt crystallization. The study of the mechanisms shows that the

Fig. 1. Monte Kali in Germany (Source:Vesna Pungercar).

surface's inclination can influence the growth of salt crystals on the surface.

A literature review found that salt accumulation on the surface can be analyzed using different methods [53–64]. The most used aim at visual inspection [53,58,60,65], chemical analysis (X-ray diffraction, Gravimetric Analysis, Ion Chromatography, Fourier Transform Infrared Spectroscopy) [55,59,64,66], surface analysis (Scanning Electron Microscopy, Energy Dispersive X-ray spectroscopy) [62,67], material analysis (moisture testing, porosity testing, mechanical testing) [54,56,57,68] and standardized testing methods outlined by ASTM standards [61]. The salt deposits can be visually inspected and compared with other surfaces [53,58,60, 65]. However, the analysis is subjective and needs to give more qualitative results. Chemical analysis includes the investigation of weighing samples and identifying crystalline compounds, ions, or molecular structures [55,59,64,66]. However, it cannot provide a complete picture of efflorescence across large surfaces. The surface analysis also gives detailed information at the microscopic level, but due to magnification issues, the analyzed surfaces are always small and can only be generalized for part of the surface [62,67]. More indirect information about the efflorescence provides material analysis [54,56,57,68] but does not directly show the efflorescence's effect. Standardized testing methods can sometimes be high inclination and only consider some different conditions [61]. Therefore, analyzing methods should have a microscopic level for defining the chemical composition and a macro level for determining the amount of efflorescence. Thus, the use of imaging methods as in this paper can better address the heterogeneity of the salts deposits and distribution across the surfaces.

Our experimental study aims to evaluate the efflorescence of salt-concrete material at different surface inclinations. This acknowledgment would help to design salt-concrete wall panels with a maximum salt efflorescence for potential enchancement of respiratory health as well as evaluate the capabilities and limitation of non-destructive imaging methodologies for salts efflorescence evaluation. The experimental results will show the potential of using a high amount of salt waste by reducing cement usage in building materials and improving the understanding of optimized surface design in indoor construction applications.

2. Materials and methods

An optimal surface that absorbs as much heat as possible and is health-promoting should have the largest projected surface area. This means the panels should have a textured surface instead of a low inclination one. Inspirations for surface structuring were found in nature. In this research project, the surface of the human small intestine was used as a model, which achieves a large surface area through the formation of so-called intestinal villi.

To determine the optimal surface design of the panels, the salt crystallization at different surface inclination angles was systematically investigated by Confocal laser scanning microscopy (CLSM) and Macro X-ray Fluorescence imaging (MA-XRF). Our research contributes to better understand the formation of salts efflorescence on salt-concrete materials, which helps to give guidelines for optimizing and designing indoor wall panels (see Fig. 2). The Fig. 2 illustrates a structure inspired by the human intestine, characterized by a small external surface area but an extensively large internal surface area. This unique configuration made it an ideal template for experiments aimed at enhancing the surface areas of specimens.

2.1. Materials

2.1.1. Salt-concrete mixture

The salt-concrete mixture was predefined from previous research due to its superior mechanical performance [69]. Materials selected for the salt-containing mixtures included Portland limestone cement (CEM II/A-LL 42.5 R, manufacturer: Heidelberg Materials Cement), sand (CEN standard sand according to DIN EN 196, manufacturer: Normensand GmbH 6), distilled water, and salts from potash (distributer: Diacleanshop and desalination production (distributer: Diacleanshop). The mixture paste was prepared according to standard DIN 196–1, with a water-to-cement ratio of 0.70 and a cement-to-sand ratio of 1:3 (see Table 1).

In this study, XRD analysis was not performed because the chemical composition of the salts was obtained from existing literature (see Table 2). Additionally, the industry was unwilling to provide the actual salt waste for direct analysis. As a result, we reproduced the salt mixtures based on their known chemical compositions from published sources, ensuring that the materials used in the study were representative of real industrial salt waste. Instead of conducting XRD, we relied on XRF analysis to confirm the elemental composition of the synthesized salt mixtures. This approach allowed us to study the influence of these salts on concrete mixtures while maintaining consistency with industrial compositions, despite the lack of direct industrial samples.

The chemical composition of cement, sand, and the two different salt waste materials was determined using Inductively Coupled
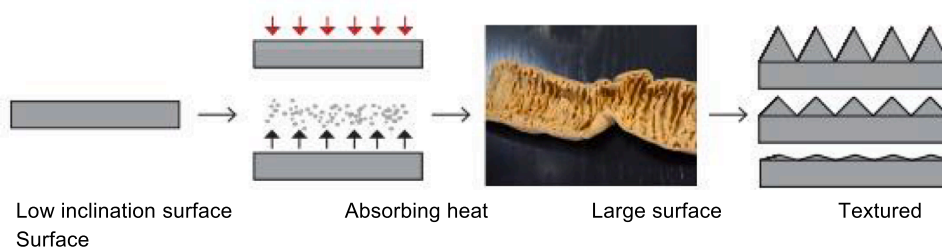

Low inclination surface   Absorbing heat   Large surface   Textured
Surface

Fig. 2. The concept of increasing surface area.

Table 1

Salt-concrete mixture proportions (kg/m^3).

Mixture	Cement	Desalination salts	Potash salts	Sand	Distilled Water
Desalination salt concrete (DS)	258	343		772	180
Potash salt concrete (PS)	258		343	772	180

Table 2

Chemical composition of salt waste from desalination and potash production [70,71].

Chemical composition	Potash production [wt%] [70]	Desalination [wt%] [71]
NaCl	94.8	77.0
KCl	2.6	2.0
MgCl2	0.8	10.0
MgSO4	0.2	7.0
CaSO4	-	4.0

Plasma Optical Emission Spectrometry (ICP-OES) Avio 500 ICP-OES, PerkinElmer. The results of the chemical analysis show that the examined cement is as expected primarily composed of CaO, SiO_2, Al_2O_3, Fe_2O_3, and SO_3, while the sand is mainly composed of Al_2O_3 and SiO_2. The characteristic salts from the desalination plants and potash production mostly contain Cl, Na, K, Na_2O, and MgO (see Table 2). The term SO₃ (IC]) refers to the sulfur trioxide (SO_3) content measured using Ion Chromatography (IC) and SO₃ (OES) represents the sulfur trioxide content determined through Optical Emission Spectroscopy (OES). The notation Na₂O-ä indicates a specific variation in the measurement of sodium oxide (Na_2O), involving a correction factor.

The cement and salt particle sizes (from desalination plants) were determined using a laser granulometer (see Fig. 4). For this purpose, the samples were dispersed in isopropanol and then measured using laser diffraction. The grain size distribution of CEN norm sand (from Normensand GmbH), based on the producer product description, ranges between 0.08 and 2.00 mm.

Table 4 presents the particle size distribu

tion (d10, d50,dD90) for CEM II/A-LL 42.5 R cement, desalination salts, and CEN norm sand. The CEN norm sand has the largest particles, with d50 = 400 µm. In contrast, the desalination salts (d50 = 16.4 µm) and cement (d50 = 8.7 µm) have much finer particles. The d90 values show that 90 % of CEN norm sand particles are smaller than 120 µm, whereas the desalination salts and cement have d90 values of 40.1 µm and 31.1 µm, respectively, confirming that sand has the coarsest grain structure. The chemical compositions of the DS and PS salts differed, but the grain size distributions provided by the producer were the same across the different compositions. Therefore, only one desalination salt mixture was analyzed to verify the producer's information regarding grain size distribution. The particle size distribution of CEN norm sand was taken from the producer's information, as it was predefined and supplied by the manufacturer.

2.1.2. Preparation of mock-ups

Sample preparation was carried out following a 7-step procedure (see Fig. 5). The preparation procedure of the paste involved weighing (Step 1) of each component. It is followed by mixing using a mechanical mixer Siemens TD 200 to ensure the homogeneity of the mixture (Step 2). The paste mixture was distributed into the mold compartments (Step 3). The mold compartments used for shaping the paste samples were custom-designed and fabricated using a laser cutter to create the prototype form. This means that the molds were specifically crafted to fit the intended sample dimensions and experimental requirements, ensuring precision and consistency in

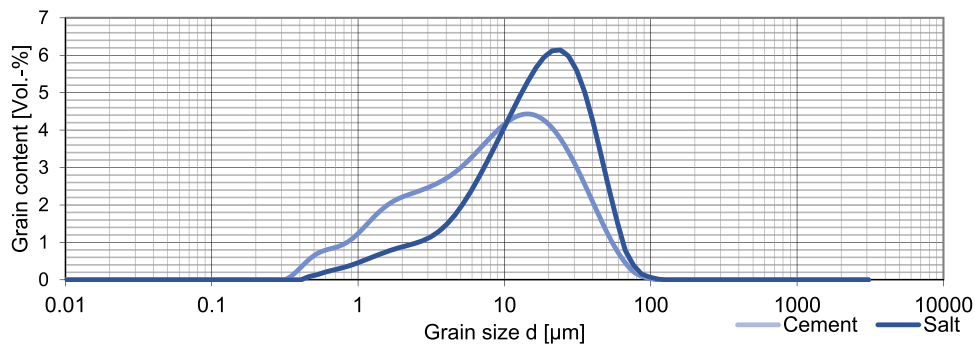**Fig. 3.** Materials for potash salt–concrete mixture.

Fig. 4. Grain sizes of cement and desalination salts.

Table 3
Chemical composition of materials (% by weight).

	CEM II/A-LL 42,5 R	Normsand	Potash salts (PS)	Desalination salts(DS)
SO_3 [IC]	3.07	0.00	0.00	0.00
SO_3 [OES]	3.32	0.22	0.46	4.96
Sulfide	0.04	0.00	0.00	0.00
Cl^-	0.00	0.00	58.97	53.35
Na^+	0.00	0.00	36.85	31.49
K^+	0.00	0.00	1.58	1.31
Ca^{2+}	0.00	0.00	0.01	1.07
Mg^{2+}	0.00	0.00	0.30	2.48
Na_2O	0.29	0.20	49.64	42.43
K_2O	0.63	0.78	1.90	1.57
Na_2O-ä	0.71	0.71	50.89	43.46
CaO	62.25	0.10	0.02	1.50
MgO	0.80	0.09	0.49	4.12
Fe_2O_3	1.29	0.53	0.00	0.00
Al_2O_3	3.57	1.61	0.00	0.01
SiO_2	20.08	95.86	0.00	0.00
P_2O_5	0.18	0.07	0.02	0.05
BaO	0.02	0.02	0.00	0.00
SrO	0.17	0.00	0.00	0.01
MnO	0.04	0.01	0.00	0.00
TiO_2	0.21	0.06	0.00	0.00
Cr_2O_3	0.01	0.00	0.00	0.00
V_2O_5	0.01	0.01	0.00	0.00
ZnO	0.01	0.00	0.00	0.00

Table 4
Particle size distribution.

	CEM II/A-LL 42.5 R, (µm)	Desalination salts (µm)	CEN norm sand (µm)
d10	1.3	3.1	900
d50	8.7	16.4	400
d90	31.1	40.1	120

sample preparation. During the filling process (Step 4), the paste undergoes gentle poking to facilitate the expulsion of air, thereby reducing the likelihood of pore formation. Following this step, the samples undergo a drying period at 20°C and 50 % relative humidity in the climate chamber for 24 hours (Step 5) before being carefully de-molded (Step 6). Upon demolding, the samples are sealed with tape (Step 7), leaving only the observed surface exposed to air to promote salt crystallization predominantly on the surface. These prepared samples are then stored under specified conditions for 27 days at 20°C and 50 % relative humidity in a climate chamber (Step 8), adhering to the standard curing time for cement to allow for comprehensive analysis and observation. It is essential to note the difficulty in controlling and avoiding pores on the samples while also acknowledging that the edges of the samples may exhibit relative brittleness at the time of demolding.

To study how the inclination and salt chemical composition would affect the crystal growth on the cement surface, two series of samples (Set A and Set B) that are different in volume were designed (seeFig. 6). The initial series (Set A) comprised samples with a consistent inclined surface measuring 10 cm in width and 10 cm in length, and different cm in height. The second series (Set B) featured samples of identical dimensions, measuring 10 cm in width, 10 cm in length, and 2 cm in height. Each series encompassed six
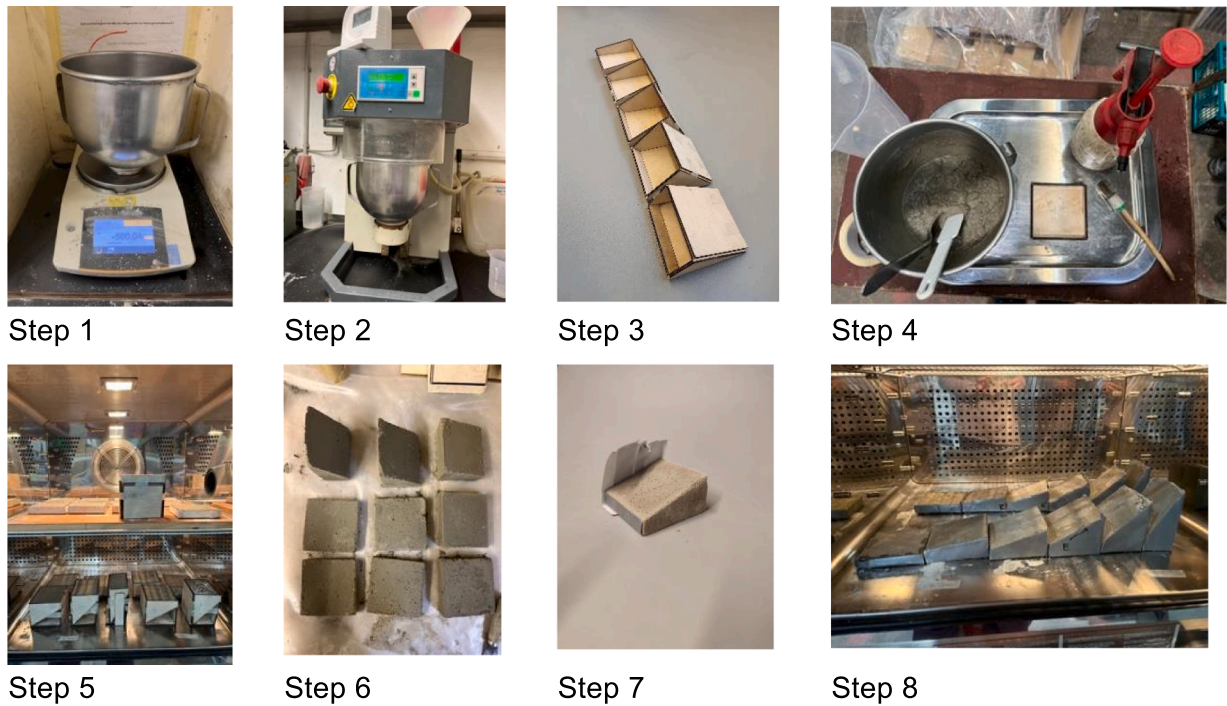
Fig. 5. A series of photos showing the sample preparation process: Step 1: Weighting, Step 2: Mixing, Step 3: Creating molds, Step 4: Filling the molds, Step 5: Drying in a climate chamber for 24 hours. Step 6: Demolding, Step 7: Sealing the samples, Step 8: Drying the samples in a climate chamber for 27 days.

Fig. 6. Figures explaining the mold compartments: (a) Set A and (b) Set B.

samples with inclinations (θ) at 0°, 10°, 20°, 30°, 45° and 60°. All samples with inclination from 0 to 30° are defined as low inclination surfaces, and the inclination between 30 and 60° as high inclination surfaces. Photos were captured perpendicular to the surface by maintaining a constant observed area, facilitating more accessible surface analysis. Fig. 6 shows the two samples sets.

2.1.3. Methods

CLSM and MA-XRF (Fig. 8) were employed for investigating the mock ups surfaces. Both methods are non-destructive and do not require the removal of samples and permit the analysis without contact with the surface of the specimen. CLSM was expected to reveal higher roughness at the upper points of the surface, as increased crystallization is anticipated to occur there, according to the literature. Macro X-ray Fluorescence was expected to show that the crystallization of Cl-based salts varie with the material mixture (potash and desalination salts) and inclination on the surface of samples. The results of both methods are shown and discussed below.

CLSM enables the collection of detailed surface information such as porosity, wear, cracking, and roughness across various materials, especially cement-based materials [72–74]. In this research study, a Confocal Laser Scanning Microscopy (VK-X100-M-D) from Keyence was utilized to analyze the surface roughness on two measurement areas of each sample. The microscopy employed a red laser
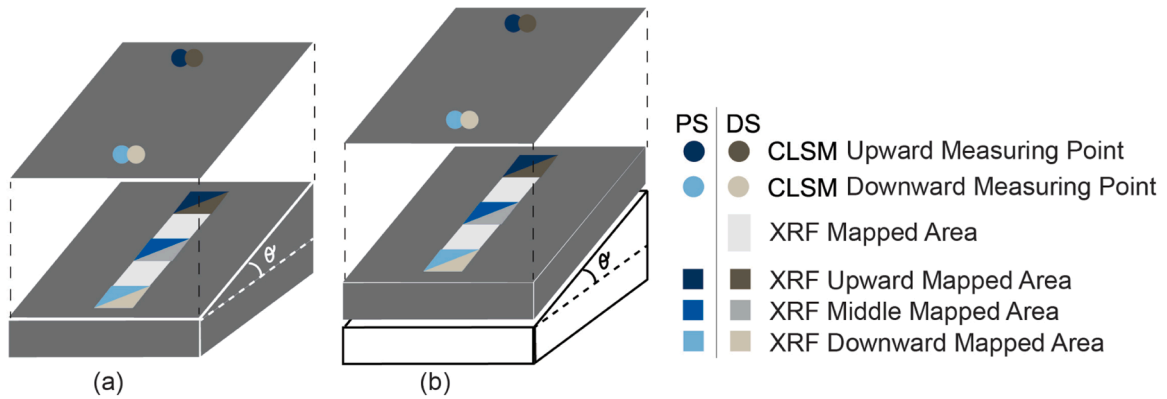
Fig. 7. (a) Set A; (b) Set B. CLSM Measurements are shown as the upper surface at both sets with the position of the measurement point of dark blue (PS Upward Measuring Point), bright blue (PS Downward Measuring Point), dark gray (DS Upward Measuring Point) and bright gray (DS Downward Measuring Point). MA-XRF measurements are shown as downward surfaces on the samples with rectangular surfaces in the middle of the sample. Three areas at MA-XRF are evaluated: dark blue (PS Upward Mapped Area), bright blue (PS Middle Mapped Area), very bright blue (PS Downward Mapped Area), dark gray (DS Upward Mapped Area), bright gray (DS Middle Mapped Area) and very bright gray (DS Downward Mapped Area).

Fig. 8. Data collection tools, left: Scanning Confocal Microscopy, suitable: Macroscopic X-ray Fluorescence.

(685 nm) as its light source. Data were collected with objective lenses with a 5x magnification in which each scan covered a viewing measurement range of 2700 μm horizontally and 2025 μm vertically. Data collection was facilitated through the VK Aufname-Modul and VK Mulitfile Analyser software, enabling the generation of detailed surface maps for analysis. One measurement area was in the upper part, and one was in the lower part of the samples. In this experimental study, CLSM measurements were conducted on two
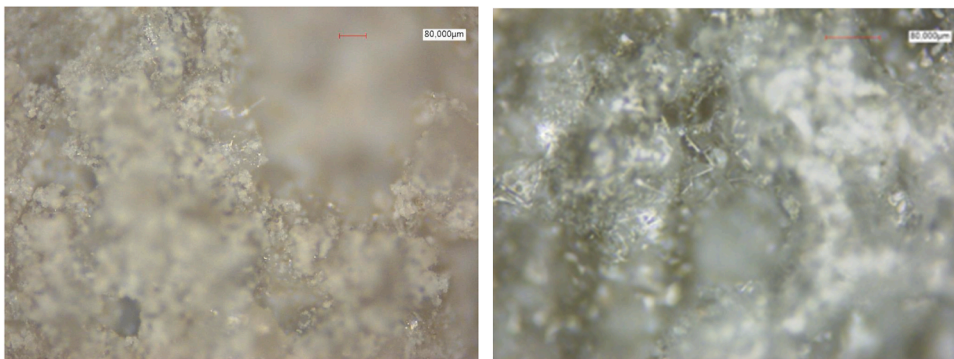

Fig. 9. Microscopic view showcasing the growth of salt crystal. Left: With 10x magnification. Right: with 40x magnification, the cubic crystal structure grown in different directions can be observed.

distinct areas.

MA-XRF analysis were performed with an ELIO spectrometer (Bruker) equipped with an Rh source operating at 30 kV and 80 µA. The focal spot size is of 1 mm, with an acquisition time of 60 s for punctual analysis and 1 s/px for mapping (total of 320 measurements/px per mapping). The measurements are acquired at a distance of one cm from the sample's surface. The Elio spectrometer has a two-laser-based system that permits the optimisation of the measurement conditions in terms of X-ray source and detector geometrical alignment. The spatial distributions of the elements were obtained using Elio Bruker software. Neither helium flow nor filters were used. However the use of Helium could permit a higher sensitivity to light element, it cannot be used during mapping measurements. Semi-quantitative data evaluation was performed with ArtTAX-Ctrl software (Intax). The instrument allows the detection of elements with $Z \geq 11$ (Na). In this paper, Chlorine (Cl) and Potassium (K) were considered as marker-elements of the added salts. All the intensities shown below for up, middle and downward areas are mean values of 60 measurements/pixel. To permit comparison between the different samples/sets, signal intensities were normalized using the signal of the Rh (emission line Kα1 20.216 keV).

3. Results and discussion

Based on macroscopic observation, salts efflorescence is clearly visible on the surface of all the mockups sets after curing. Fig. 9 shows the concrete surface under the optical microscope at a magnification of 10x (Fig. 9, left) and 40x (Fig. 9, right). Cubic crystal shapes indicate the presence of Cl-based salts formation. While the varied growth directions of the salt could influence the surface topography in 2D, the volume of salt efflorescence can be expressed in terms of surface roughness, which values can be precisely measured using 3D laser confocal microscopy and used as parameter to compare the different specimen.

3.1. Surface roughness evaluation

The surface roughness values collected using confocal microscopy are summarized in Table 5 and Fig. 10, illustrating the changes in surface roughness of the concrete after curing at different dryinginclination. The results indicate that at the top measurement point, the surface roughness is higher than the bottom position at both samples and material mixtures. This is in line with the results of Nachshon et al., where the increase of efflorescence at great inclination has been explained because of the greater gravity [51].

In Set A, the surface roughness is:

- 9.14 % higher (from 23.449 µm to 25.593 µm) at the upwards measurement point
  compared to the downwards measurement point for the PS mixture.
- 11.65 % higher (from 19.703 µm to 22.303 µm) at the upwards measurement point
  compared to the downwards measurement point for the DS mixture.
- max by 25.593 µm at the upwards measurement point at the DS mixture.
- min by 19.703 µm at the downward measurement point at the PS mixture.
  In Set B, the surface roughness is:
- is up to 31.01 % higher (from 15.874 µm to 20.800 µm) at the upward measurement
  point compared to the downward measurement point for the PS mixture
- 21.95 % higher (from 16.975µm to 21.752 µm)) at the upward measurement point
  compared to the downward measurement point for the DS mixture.
- max by 21.752 µm at the upward measurement point at the PS mixture
- min by 15.874 µm at the downward measurement point at the PS mixture.

There is also a difference between sample sets A and B. The highest value in Set A is observed at the upward measurement point at DS mixtures by 25.593 µm. The highest value in Set B is observed at the upward measurement point at PS mixtures by 21.752 µm.

3.1.1. Surface roughness: low inclination surfaces versus high inclination surfaces

The roughness of the high inclination and low inclination surfaces is presented in Table 5 and Fig. 11. Analysis indicates that the

Table 5
Average Surface Roughness values of two salt mixtures (DS and PS) for sets A and B.

Salt mixture	Position of measurement	Average Surface roughness (µm)	Standard Deviation
Set A			
PS	Upwards	25.593	8.954
	Downwards	23.449	6.134
DS	Upwards	22.303	4.862
	Downwards	19.703	3.926
Set B			
PS	Upwards	20.800	20.159
	Downwards	15.874	16.378
DS	Upwards	21.752	15.986
	Downwards	16.975	13.029

Table 6

The evaluated topography and rendered 3D model of Set A_PS Upward Measurement at three different surface inclinations (0°, 30°, 60°) with CLSM.
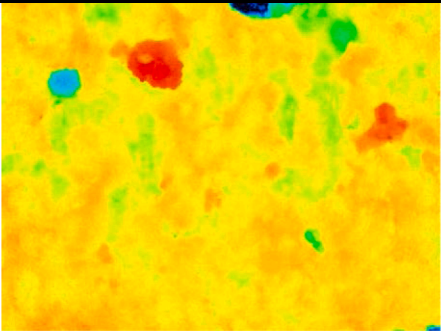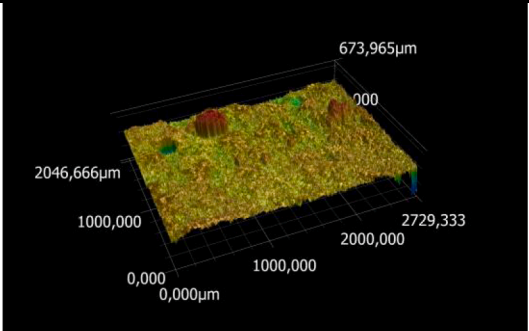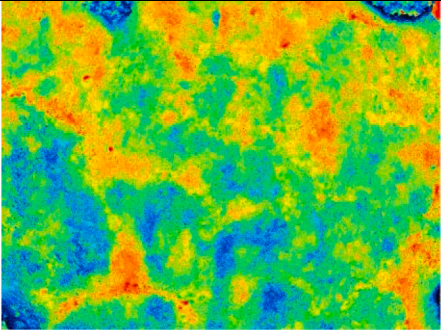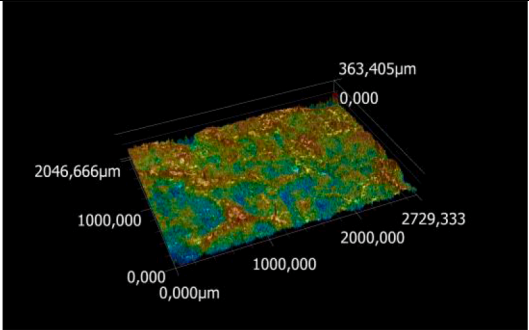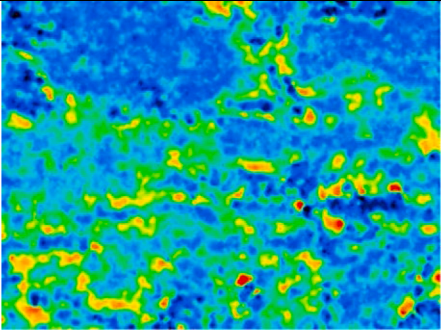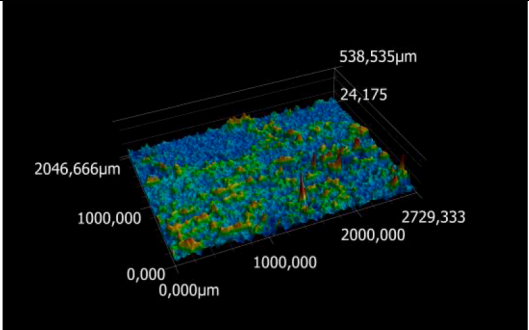
Surface Inclination	Topography	Rendered 3D
0°		
30°		
60°		

Table 7

Surface roughness between low inclination and high inclination surfaces for the DS and PS mixtures' upward and downward measurement values for sets A and B.

Set A				
Salt mixture	Inclination	Position of measurement	Average Surface roughness (μm)	Standard Deviation
PS	0–30°	Upwards	3.82	0.034
	0–30°	Downwards	3.78	0.017
	30–60°	Upwards	37.82	12.107
	30–60°	Downwards	27.93	15.321
DS	0–30°	Upwards	16.09	11.305
	0–30°	Downwards	6.50	4.740
	30–60°	Upwards	27.42	20.367
	30–60°	Downwards	27.46	8.517
Sample Set B				
PS	0–30°	Upwards	21.89	6.401
	0–30°	Downwards	18.91	5.664
	30–60°	Upwards	29.30	10.874
	30–60°	Downwards	27.99	0.266
DS	0–30°	Upwards	21.29	7.436
	0–30°	Downwards	16.89	3.337
	30–60°	Upwards	23.32	0.840
	30–60°	Downwards	22.52	1.926

surface roughness for the high inclination surface (inclined at 30–60º) was always higher than that of the low inclination surface (inclined at 0–30º) across most measurements. Table 5 shows the evaluated topography and rendered 3D model of Set A_PS Upward Measurements as examples for visual validation at different surface inclinations. Set A, with higher inclination, showed more significant differences between the surfaces' minimal and highest measured points (more variation in colors – from blue to yellow). Lower inclination and lower surface roughness were observed at 0° inclination, with more consistent colors ranging from yellow to red.

For Set A, the surface roughness for PS and DS mixtures is always higher than the low inclination surface roughness. Also, an increase in the surface roughness at the upward in comparison to downward measurement points is noted within both material mixtures. The surface roughness is:

- 90 % higher (from 3.78 μm to 37.82 μm) at the high inclination upwards measurement point compared to the low inclination upwards measurement point for the PS mixture.
- 88 % higher (from 3.82 μm to 27.93 μm) at the high inclination upwards measurement point than the low inclination upwards measurement point for the DS mixture.
- max by 26 % at the upwards measurement point compared to the downwards measurement point at the PS mixture (30–60°).
- about 0 % at the upwards measurement point compared to the downwards measurement point at the DS mixture (30–60°).

Set B's differences in surface roughness for PS and DS between high inclination and low inclination surfaces are not as high as in Set A. The surface roughness is:

- 25 % higher (from 21.89 μm to 20.80 μm) at the high inclination upwards measurement point compared to the low inclination upwards measurement point for the PS mixture.
- 9 % higher (from 15.975μm to 22.753 μm) at the high inclination upwards measurement point compared to the low inclination upwards measurement point for the DS mixture.
- max by 201 % at the upwards measurement point compared to the downwards measurement point at the DS mixture (0–30°).
- min by 3 % at the upwards measurement point compared to the downwards measurement point at the DS mixture (0–30°).

3.2. Sample/surface characterization: elemental analysis

The elements detected by Macro-XRF in both sample sets include Si, S, Cl, K, Ca, and Fe, with minor signals of Sr and Ti. It is important to note that the depth of XRF measurement varies based on the energy of the element and the density of the matrix. For a concrete matrix, the densities are 1882 kg/m^3 for DS and 1950 kg/m^3 for PS. The penetration depths for Cl analysis are 1.77 mmfor DS and 1.71 mmfor PS[75]. This indicates that we were able to fully penetrate the salt efflorescence (maximum thickness of 2 mm) on the surface and detect signals from the saturated concrete block.

3.3. Effect of the salts admixtures

PS and DS mixtures showed different crystallization amounts on the surface. Fig. 11 shows that only once, for the surface roughness of PS concrete at 0–30° inclination, the values are lower than those of the DS concrete mixture. This salt accumulation pattern suggests a chemical composition affecting salt crystallization. It is essential to emphasize that DS salts have about 11 times more SO$_3$ (in PS 0.46 wt%, in DS 4.96 wt%) and about 8 times more MgO (in PS 0.49 wt%, in DS 4.12 wt%) than PS salts.

A salt concrete mixture containing higher levels of SO$_3$ and Mg can contribute to more stable matrix [76–78] and could also help to reduce efflorescence. Sulfur trioxide (SO$_3$) is introduced into cement through gypsum (CaSO$_4 \cdot 2H_2O$) to regulate hydration [79–81]. It

Table 8

Surface roughness values for low inclination and high inclination surfaces of DS and PS mixtures' upward, middle, and downward measurement for sets A and B.

Cl					
		Mean (x = 60)	S(x = 60)	Min	Max
Down	20240430_PS_deg0	47,4	12,3	25,6	71,3
	20240403_A_PS_60deg	56,8	19,5	29,3	150,5
	20240403_B_PS_60deg	57,3	15,3	31,1	91,9
Middle	20240430_PS_deg0	45,6	11,1	31,0	74,8
	20240403_A_PS_60deg	59,4	18,9	36,2	141,0
	20240403_B_PS_60deg	52,3	23,0	25,1	167,3
Upper	20240430_PS_deg0	42,9	13,1	15,2	95,4
	20240403_A_PS_60deg	56,5	15,3	37,0	116,3
	20240403_B_PS_60deg	58,9	14,8	38,5	105,8
K					
		Mean (x = 60)	S(x = 60)	Min	Max
Down	20240430_PS_deg0	8,6	2,3	4,5	13,1
	20240403_A_PS_60deg	2,7	1,5	1,1	9,8
	20240403_B_PS_60deg	7,7	2,5	2,2	15,3
Middle	20240430_PS_deg0	8,3	2,4	3,5	15,9
	20240403_A_PS_60deg	1,5	0,7	0,5	4,0
	20240403_B_PS_60deg	7,2	3,0	2,8	18,0
Upper	20240430_PS_deg0	8,3	2,8	3,0	20,7
	20240403_A_PS_60deg	2,7	1,5	1,0	7,3
	20240403_B_PS_60deg	7,3	2,9	2,7	14,3
Cl					
		Mean (x = 60)	S(x = 60)	Min	Max
Down	20240430_DS_deg0	48,8	15,7	24,4	113,0
	20240403_A_DS_deg60	50,6	14,2	25,0	110,9
	20240403_B_DS_60deg	34,7	11,7	17,4	64,9
Middle	20240430_DS_deg0	48,5	13,0	28,1	82,1
	20240403_A_DS_deg60	56,9	17,5	31,4	114,7
	20240403_B_DS_60deg	34,6	11,1	14,6	63,0
Upper	20240430_DS_deg0	40,5	9,6	26,5	65,6
	20240403_A_DS_deg60	54,0	22,1	20,5	132,1
	20240403_B_DS_60deg	29,4	10,8	13,3	66,5
K					
		Mean (x = 60)	S(x = 60)	Min	Max
Down	20240430_DS_deg0	8,7	3,0	4,6	23,6
	20240403_A_DS_deg60	2,1	0,8	0,8	4,8
	20240403_B_DS_60deg	7,2	2,6	2,8	13,6
Middle	20240430_DS_deg0	8,9	2,6		
	20240403_A_DS_deg60	3,3	1,3	1,2	5,8
	20240403_B_DS_60deg	7,3	1,9	4,5	12,6
Upper	20240430_DS_deg0	9,3	2,0	2,5	18,7
	20240403_A_DS_60deg	7,3	3,3	3,8	23,7
	20240403_B_DS_60deg	6,1	2,4	5,4	14,5

plays a key role in controlling the reaction of tricalcium aluminate (C_3A). The right amount of SO_3 ensures proper ettringite formation, enhancing early strength and preventing cracks [81]. In blended cements, such as those with fly ash or silica fume, SO_3 helps maintain an alkaline environment [80]. This promotes further hydration, leading to a denser structure and improved long-term durability. A well-balanced SO_3 content lowers permeability, reducing the movement of salts and minimizing efflorescence [79]. However, excessive SO_3 can cause expansion and structural issues [80]. Mg contributes to chemical binding by promoting the formation of magnesium-aluminum layered double hydroxide (Mg-Al LDH), which can trap ions more effectively. This reduces the availability of free chloride, one of the main contributors to salt efflorescence, thereby limiting its migration to the surface [76]. However, under humid conditions, the presence of sulfates and MgO in concrete can lead to expansive phenomena (increase of the volume and internal stresses) that influence negatively the durability of concrete [82,83].

Since XRD measurements were not conducted, CemGEMS simulations were used as an alternative to predict the expected hydration phases and chemical interactions in three cementitious systems: plain cement (without added salts), cement with desalination salts, and cement with potash salts (see Table 1, Table 2, Table 3). Simulations confirmed higher SO_3 and MgO levels in DS salt mixtures promoted gypsum and ettringite formation. In contrast, PS (Fig. 12) mixtures exhibit lower sulfate binding and greater efflorescence potential. Brucite (Mg(OH)$_2$) formation is more pronounced in DS mixtures, indicating that the hydration of MgO can contribute to increased expansion risks under humid conditions. In contrast, PS mixtures exhibit lower Brucite formation, suggesting a reduced potential for expansion-related issues. DS mixtures have a lower aqueous phase volume, where more ions could be chemically bound, while PS mixtures retain more free ions and could increase efflorescence formation. These results align with MA-XRF findings, where chloride distribution is more uniform in DS mixtures and localized in PS mixtures. The simulations of PS mixture could stabilize chlorides through Friedel's Salt, but would probably not fully prevent their migration. The findings confirm that balancing SO_3 and
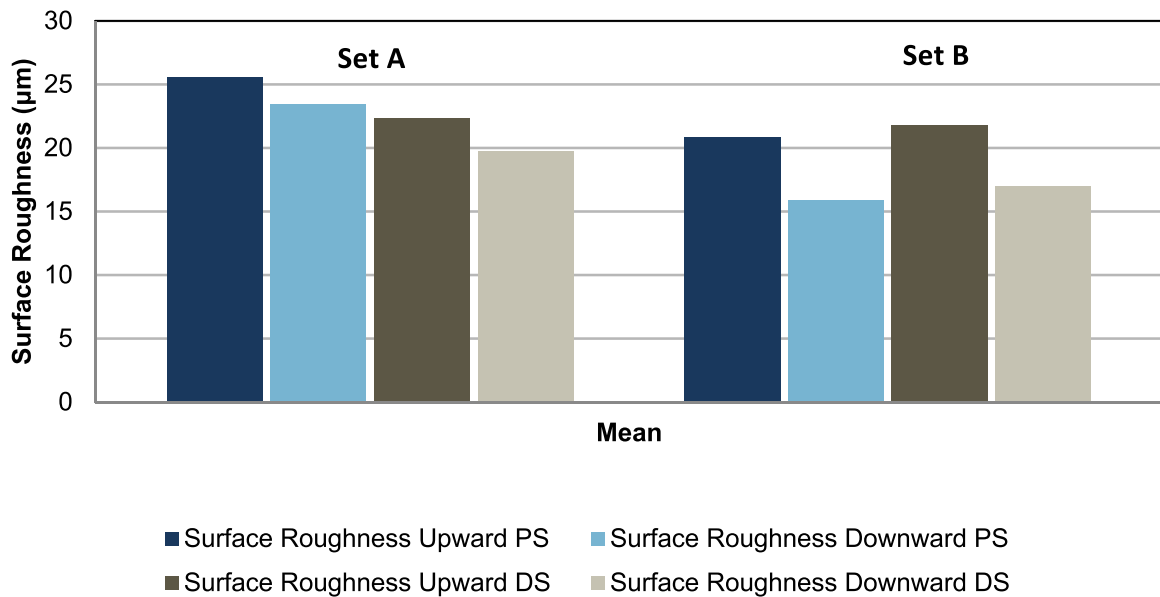
Fig. 10. Surface Roughness for the upward and downward measurement values of DS and PS mixtures for Set A and B.

MgO content is crucial to minimizing efflorescence while preventing expansion-related damage. These computational results strongly support the experimental observations.

As a result, the Fig. 12 shows the XRF mapping of the mock-ups with a low inclination surface (0°) in comparison to the specimen with a 60° inclination for both set A and B of DS and PS concrete admixtures. In the mapping, red indicates higher counts/pixel values (signal intensity) for the selected element/energy line, while dark blue represents lower signal values.

When comparing the maximum signals detected for Cl in the low inclination samples for both salt-concrete admixtures, the values are comparable (max $\geq$ 3000 counts). The signal detected for K, however, is slightly lower for the low inclination surface of the PS-concrete admixture (max $\geq$ 700 counts). If we observe the distribution of the presence of Cl-based salts, these are more heterogeneously distributed for the DS-samples. Most areas shows low signals (areas mostly green and blue coloured) in comparison with the PS-admixture where the signal are hiher (areas mostly yellow-red coloured).

Furthermore, in the mappings, it is possible to observe that the Cl-based compounds are quite uniformly distributed. The K mapping permits to observe the distribution of KCl salts.

3.4. Effect of the salts/concrete volume

The experimental results for CLSM are presented in Fig. 10 and Fig. 11. It can be seen that all maximal values were measured in Set A (25.593 µm in PS Upwards, 23.449 µm in PS Downwards, 22.303 µm in DS Upwards, and 19.703 µm in DS Downwards). Set A has, in comparison to Set B, a minimum increase in the mass up to 42 % at an inclination of 10° and a max 108 % at an inclination of 60°. The reason for higher values at Set A found in the literature is that a higher amount of salt can be presented with more mixture mass. More salt in the mixture increases the potential for a higher density of salt crystals on the surface [84].

According to the CLSM results, the XRF mean signals detected for Cl for set A are higher than set B, confirming that the volume affects the migration of salts.

3.5. Effect of the surface inclination

As shown in Fig. 11 and Table 5 with CLSM, the average surface roughness values are between 25 % and 90 % higher at high inclination inclination (30–60°) than at low inclination (0–30°). The same tendency is observed for both sets (A and B) and both material mixtures. Concerning the inclination, different researchers attributed the reason for more efflorescence to the distribution of capillary water with the material and evaporation on the inclined surface [51,84]. Low inclination surfaces were smoother, had fewer nucleation sites, and crystals grew more uniformly than on surfaces with high inclination. these highly inclined surfaces showed more irregularities and pores than the low inclination ones.

The differences in measure positions were also noted. When we took the same material and inclination, different values were measured at the upward and downward positions. As shown in Fig. 10 and Fig. 11, in most cases, the downward measurement point is performed with lower average surface roughness as the upward measurement point. Almost no difference was measured at the DS mixture (30–60°) whereas maximal difference of about 26 % at the PS mixture (30–60°). It is supposed that salt crystallized in higher amounts on the upper part of the inclined surface due to the accumulation of water and solute at the lowest part [51]. Solute transport
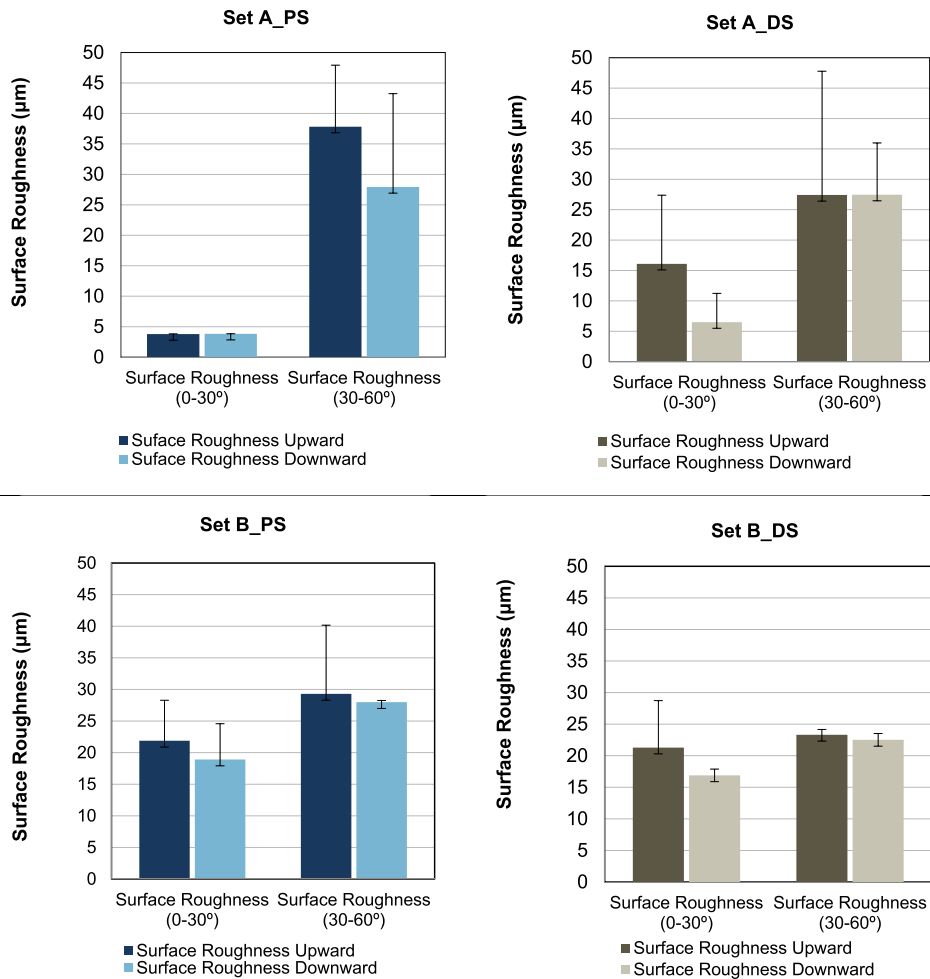
Fig. 11. Surface roughness between low inclination and high inclination surfaces for the Upward and Downward measurement values of DS and PS mixtures for sets A and B.

parallel to the slope is fast enough that salt crystallizes crystalizes at the upper part, but in the lower region, it can not. When the material does not have much water content, the solute is no longer transported to the upper part; salt crystals also occur in the lower region. However, it is still less than the amount on the upper part.

Considering the mapping in Fig. 12, the maximum counts detected for the Cl signal significantly increase from low inclination samples to inclined samples (60°) for both salt-concrete admixtures. However, in the mapping for the 60° inclination, it is unclear whether there are differences between the upper, middle, and lower areas.

In Fig. 13, the graphical representation illustrates the mean count values normalized by the Rh signal for 60 measurements in three distinct areas: upper, middle, and downward. If we examine the PS-admixture graph for Cl, the values for the samples of Set A and Set B, inclined at 60° are higher than those for the low inclination sample. A slight increase in the count values is observed between the downward and upper areas. In the DS-admixture graph for Cl, the values for the Set B sample, inclined at 60°, are higher than those of the low inclination sample, similar to the PS-admixture results. In contrast, Set A shows significantly lower values compared to all the other samples analyzed. This observation could align with previous findings [32,78,85] that indicate higher porosity in similar samples, which could lead to increased noise in X-ray measurements. The resulting spectra were notably noisy, with a high background, likely due to the analysis capturing air within the pores. The presence of air within the pores of a sample can interfere with the X-ray measurement, leading to scattering and background noise in the spectra. Interestingly, in the upward areas, both the values of Cl for DS and PS admixtures of Set A and Set B show convergence. This can be attributed to the fact that the thickness or concrete volume becomes comparable for both sets in the upper region.

When considering only the K values, thus those from KCl salts, the behavior of the data is similar for both the DS and PS admixtures. It appears that inclined samples exhibit lower K values, suggesting that NaCl and/or MgCl$_2$ preferentially migrate to the surface of these inclined samples. Additionally, the B set demonstrates lower K values for both the PS and DS admixtures, which correlates with the

Fig. 12. CenGEMS simulations of three cementitious systems: plain cement, cement with desalination salts and cement with potash salts.

lower volume of the samples. No clear trend regarding the effect of measurements taken at the lower, middle, and upper positions can be observed.

4. Conclusions

This paper presents a systematic experimental study on the effect of surface inclination on the efflorescence of two salt-concrete mixtures with salt compositions from potash and desalination processes. The following conclusions can be drawn based on the test results and discussions:

1. Most mixtures made with salt waste from the potash process (PS) had a higher surface roughness than that of salts from the desalination process (DS). Also, differences between measurement points on the upper and lower surface of the inclined surface were higher at PS mixtures than at DS mixtures. It is assumed that the composition of salt has a more significant effect. DS salt has a higher amount of SO_3 and MgO. The literature shows that MgO and SO_3 can react with soluble salt within the concrete so that the salt does not crystallize that much on the surface.
2. Surface inclinations are essential for the design of wall panels. We noticed that more salt crystallization developed in our experimental study in the upper parts of the inclined surface than in the lower parts. Also, with the high inclination inclination (30–60°), more salt crystallization was observed than with the low inclination surfaces (0–30°) at both materials and measurement points. The reason is in agreement with the literature where it is stated that salt crystalisation is hindered due to water capillary flow in the down part, whereas, at the upper part, the evaporation and smaller capillary flow enable a better environment for salts growing. To enhance salt efflorescence e.g. due to design wishes, the wall panel with a higher inclination and PS mixture would be the best choice.
3. CLSM and MA-XRF results showed slight discrepancies in the measurements. This can arise due to different factors. CLSM is highly sensitive to surface topography, and small inclination changes can affect measurements. MA-XRF has a greater penetration depth, and samples have a greater volume. In the future, for more reliable results, many more measurements of the same samples should be made and compared. Unfortunately, further measurements could not be performed due to limited availability of the CLSM equipment, as it was occupied by other concurrent research projects. However, multiple measurement areas will be taken in the future to ensure the results are genuinely significant and reliable.

This paper supports previous findings in the literature that the inclination of surfaces influences salt crystallization. It also shows the impact and differences between using salt waste in concrete mixtures. PS mixtures achieve a higher crystallization amount than DS mixtures. We believe salt waste composites may gain importance in building materials due to the increasing demand for drinking water and the need for sustainable waste management. However, it is important to consider that high salt content in concrete mixtures can
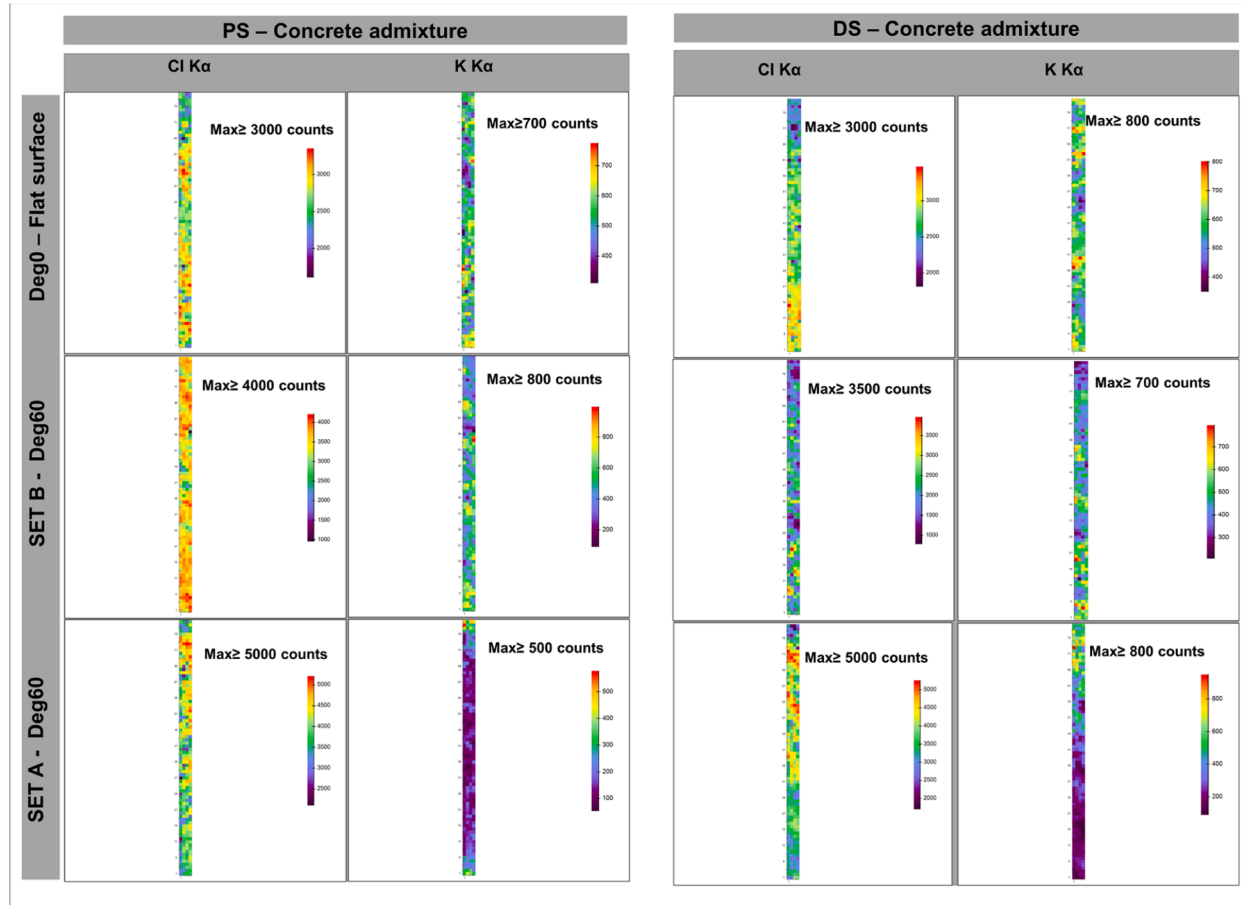
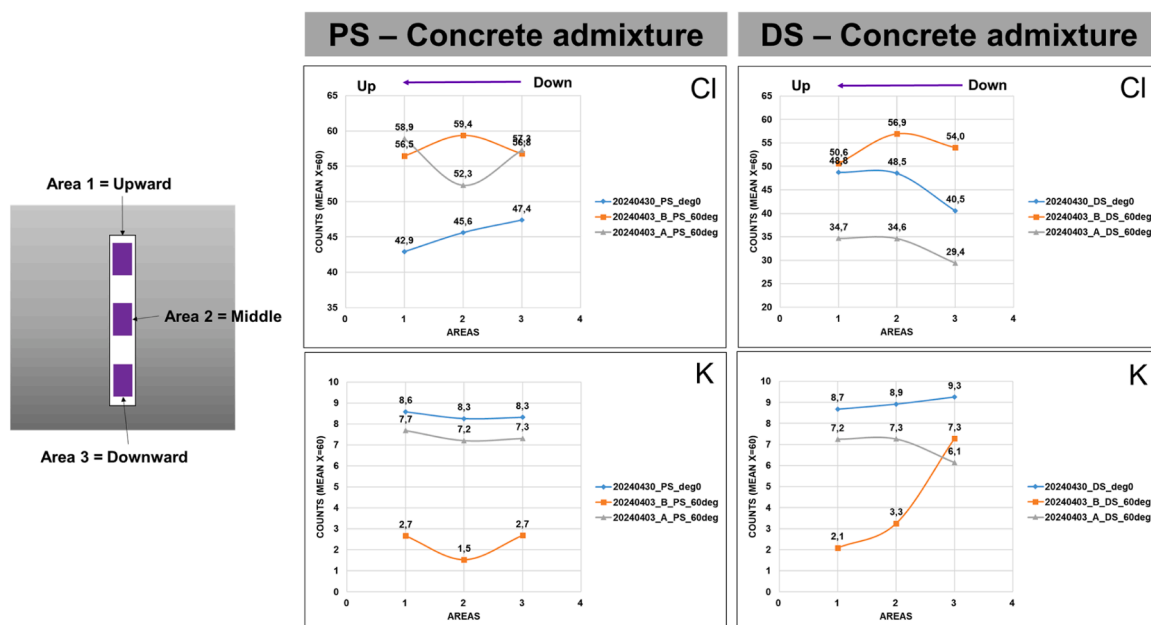**Fig. 13.** XRF mapping of the Kα line of Cl AND K, no normalized with the corresponding maximal values.

Fig. 14. A graphical representation of the mean count values (based on x = 60 measurements) for Cl and K is presented, showcasing the results for the upward, middle, and downward areas.

cause significant risks to the durability of reinforced concrete structures due to corrosion. Future research should focus on mitigating these risks through protective measures, alternative mix designs, or controlled applications where reinforcement is not a concern.

CRediT authorship contribution statement

Pungercar Vesna: Writing – review & editing, Writing – original draft, Visualization, Validation, Supervision, Software, Resources, Project administration, Methodology, Investigation, Funding acquisition, Formal analysis, Data curation, Conceptualization. **Wu Yee:** Writing – original draft, Validation, Investigation, Formal analysis. **Sessa Clarimma:** Writing – original draft, Visualization, Validation, Investigation. **Kränkel Thomas:** Writing – review & editing.

Declaration of Competing Interest

The authors declare that they have no known competing financial interests or personal relationships that could have appeared to influence the work reported in this paper.

Acknowledgements

Data availability

No data was used for the research described in the article.

References

[1] V. Pungercar, F. Musso, Salt as a building material: current status and future opportunities, TPJ 6 (2021), https://doi.org/10.15274/tpj.2021.06.02.4.
[2] E. Jones, M. Qadir, M.T. van Vliet, V. Smakhtin, S.-M. Kang, The state of desalination and brine production: A global outlook, Sci. Total Environ. 657 (2018) 1343–1356.
[3] H.M. Asfahan, M. Sultan, T. Miyazaki, B.B. Saha, A.A. Askalany, M.W. Shahzad, W. Worek, Recent development in adsorption desalination: a state of the art review, Appl. Energy 328 (2022) 120101, https://doi.org/10.1016/j.apenergy.2022.120101.
[4] A. Colas, Le sel, Presses Universitaires de France, France, 1985.
[5] J.E. Tallin, D.E. Pufahl, S.L. Barbour, Waste management schemes of potash mines in Saskatchewan, Can. J. Civ. Eng. 17 (1990) 528–542, https://doi.org/10.1139/l90-061.

[6] Ruben Ladrera, Miguel Cañedo-Argüelles, Narcís Prat, Impact of potash mining in streams: the Llobregat basin (northeast Spain) as a case study 1 (76) (2017), https://doi.org/10.4081/jlimnol.2016.1525.

[7] H. Rauche, Die Kaliindustrie im 21. Jahrhundert: Stand der Technik bei der Rohstoffgewinnung und der Rohstoffaufbereitung sowie bei der Entsorgung der dabei anfallenden Rückstände, Springer Vieweg, Berlin, Heidelberg, 2015.

[8] International Fertilizer Industry Association, Potash Case Study.

[9] Government of Canada, Natural Resources Canada: Potash facts, 2019. ⟨https://www.nrcan.gc.ca/our-natural-resources/minerals-mining/minerals-metals-facts/potash-facts/20521⟩ (accessed 24 February 2020).

[10] H. Hofmann, Untersuchungen zur Begrünung und zur Sukzession auf einer anhyddritisch geprägten Rückstandshalde der Kaliindustrie im Werraggebiet: Fachgebiet Landschaftsökologie und Naturschutz, Witzenhausen.

[11] T. Scheer, Untersuchungen zur Nutzbarkeit aufbereiteter Salzschlacke der Sekundäraluminium- Industrie als Rekultivierungs material einer Kali-Rückstandshalde: Fachgebiet Landschaftsökologie und Naturschutz am Fachbereich Landwirtschaft, Internationale Agrarentwicklung und Ökologische Umweltsicherung, Berlin.

[12] M. Cañedo-Argüelles, S. Brucet, S. Carrasco, N. Flor-Arnau, M. Ordeix, S. Ponsá, E. Coring, Effects of potash mining on river ecosystems: an experimental study, Environ. Pollut. 224 (2017) 759–770, https://doi.org/10.1016/j.envpol.2016.12.072.

[13] V. Pungercar, F. Musso, Hygrothermal performance of salt (NaCl) for internal surface applications in the building envelope, Materials 15 (2022) 3226–3235, https://doi.org/10.3390/ma15093266.

[14] V. Pungercar, M. Hutz, F. Musso, 3D print with salt, 3D printing for construction with alternative materials, digital innovations in architecture, Eng. Constr. (2023) 91–125, https://doi.org/10.1007/978-3-031-09319-75.

[15] J.P. Oleson, C. Brandon, S.M. Cramer, R. Cucitore, E. Gotti, R.L. Hohlfelder, The ROMACONS project: a contribution to the historical and engineering analysis of hydraulic concrete in roman maritime structures, Int. J. Naut. Archaeol. 33 (2004) 199–229, https://doi.org/10.1111/j.1095-9270.2004.00020.x.

[16] E. Gotti, J.P. Oleson, L. Bottalico, R. Cucitore, C. Brandon, R.L. Hohlfelder, A comparison of the chemical and engineering characteristics of Ancient Roman hydraulic concrete with a modern reproduction of Vitruvian hydraulic concrete, Archaeometry 50 (2008) 576–590, https://doi.org/10.1111/j.1475-4754.2007.00371.x.

[17] Vitruvius (Ed.), The Ten Books on Architecture. Vitruvius. Humphrey Milford. Oxford University Press. 1914., Cambridge: Harvard University Press. London: Humphrey Milford. Oxford University Press, 1914.

[18] Bauen im Salz_Entlagerung des Mülls.

[19] DBE, Planfeststellungsverfahren zur Stilllegung des Edlagers für radioaktive Abfälle Morsleben: Verfahrensunterlage (2004).

[20] W.J. van Schelven (van Schelven, William John) US3211581A, 1962.

[21] L.A. Patten US2142825A, 1937.

[22] D. Mandler, N. Lapidot, A. Buffa, G. Dikovsky, L. Rikanati (Yissum Research Development, Company of the Hebrew University of Jerusalem Ltd) US 2020/0031714 A1, 2018.

[23] Atelier Luma, Crystallization Plant | Atelier Luma, 2022. ⟨https://www.atelier-luma.org/en/projects/crystallization-plant⟩ (accessed 18 May 2022).

[24] R. Lahidji, Marbled salts, 2019. ⟨https://www.roxanelahidji.com/marbled-salts⟩ (accessed 14 August 2020).

[25] D. Manor, L. Goldberg, T. Sterngast, T. Sadowsky, Sigalit Landau: Salt years, Hatje Cantz Verlag GmbH & Company, Salzburg, 2019.

[26] E. Geboers, The Salt Project. Master thesis, 2015.

[27] M. Ganter, Salty parts - 3DP in Salt, 2011. ⟨http://depts.washington.edu/open3dp/2011/03/salty-parts-3dp-in-salt/⟩ (accessed 11 May 2020).

[28] M. Kelly, Salt, Emergence and Formation at the Dead Sea: M.Arch Thesis at University of California, Berkeley. Mastertesis, Lulu.com, Californica, USA, 2012.

[29] R. Rael, V.San Fratello, [Copy] Printing architecture: Innovative Recipes for 3D Printing, Princeton Architectural Press, New York, 2018.

[30] P. Sikora, K. Cendrowski, M. Abd Elrahman, S.-Y. Chung, E. Mijowska, D. Stephan, The effects of seawater on the hydration, microstructure and strength development of Portland cement pastes incorporating colloidal silica, Appl. Nanosci. 10 (2020) 2627–2638, https://doi.org/10.1007/s13204-019-00993-8.

[31] T.U. Mohammed, H. Hamada, T. Yamaji, Performance of seawater-mixed concrete in the tidal environment, 200528-004900 34 (2004) 593–601. https://doi.org/10.1016/j.cemconres.2003.09.020.

[32] S.A. Mangi, A. Makhija, M.S. Raza, S.H. Khahro, A.A. Jhatial, A comprehensive review on effects of seawater on engineering properties of concrete, Silicon (2020) 1–8, https://doi.org/10.1007/s12633-020-00724-7.

[33] Y.A. Sokama-Neuyam, J.R. Ursin, P. Boakye, Experimental investigation of the mechanisms of salt precipitation during CO2 injection in sandstone, C 5 (2019) 4.

[34] Z. Tang, N. Deng, Effect of salt solution on the mechanical behaviours of geopolymer concrete under dry-wet cycles, Adv. Mater. Sci. Eng. 2022 (2022) 1–9, https://doi.org/10.1155/2022/9120821.

[35] A.A. Abdullaev, K.M. Gadzhiev, A.A. Eiubova, The efficacy of speleotherapy in salt mines in children with bronchial asthma based on the data from immediate and late observations], Vopr. Kurort. Fizioter. Lech. Fiz. Kult. 5 (1993). PubMed PMID: 8266663.

[36] S.P. Beamon, A. Falkenbach, G. Fainburg, K. Linde, Speleotherapy for asthma, Cochrane Database Syst. Rev. (2001), https://doi.org/10.1002/14651858.CD001741.

[37] T. Horvath, Speleotherapy: a special kind of climatotherapy, its role in respiratory rehabilitation, Int. Rehabil. Med. 8 (1986) 90–92, https://doi.org/10.3109/03790798609166185.

[38] E.A. Puryshev, The efficacy of speleotherapy in atopic dermatitis in children, Voprosy kurortologii, fizioterapii, i Lech. Fiz. Kult. ((1994) 34–35.

[39] A.V. Chervinskaya, N.A. Zilber, Halotherapy for treatment of respiratory diseases, J. Aerosol Med. 8 (1995) 221–232, https://doi.org/10.1089/jam.1995.8.221.

[40] J. Hedman, T. Hugg, J. Sandell, T. Haahtela, The effect of salt chamber treatment on bronchial hyperresponsiveness in asthmatics, Allergy 61 (2006) 605–610, https://doi.org/10.1111/j.1398-9995.2006.01073.x.

[41] S. Horowitz, Salt Cave Therapy: Rediscovering the Benefits of an Old Preservative, Altern. Complement. Ther. 16 (2010) 158–162, https://doi.org/10.1089/act.2010.16302.

[42] R. Rashleigh, S.M.S. Smith, N.J. Roberts, A review of halotherapy for chronic obstructive pulmonary disease, Int. J. Chron. Obstruct. Pulmon. Dis. 9 (2014) 239–246, https://doi.org/10.2147/COPD.S57511.

[43] H. Lăzărescu, I. Simionca, M. Hoteteu, L. Mirescu, Speleotherapy - modern bio-medical perspectives, J. Med Life 7 (Spec 2) (2014) 76–79.

[44] J. Zajac, I. Bojar, J. Helbin, E. Kolarzyk, A. Owoc, Salt caves as simulation of natural environment and significance of halotherapy, Ann. Agric. Environ. Med 21 (2014) 124–127.

[45] K. Zehnder, A. Arnold, Crystal growth in salt efflorescence, J. Cryst. Growth 97 (1989) 513–521, https://doi.org/10.1016/0022-0248(89)90234-0.

[46] H. VILES, Salt Crystallisation in Masonry, 2012. ⟨https://www.buildingconservation.com/articles/salt-crystallisation/salt-crystallisation.htm⟩.

[47] G.W. Scherer, Stress from crystallization of salt, 200528-004900 34 (2004) 1613–1624. https://doi.org/10.1016/j.cemconres.2003.12.034.

[48] X. Jiang, S. Mu, J. Liu, Influence of chlorides and salt concentration on salt crystallization damage of cement-based materials, J. Build. Eng. 61 (2022) 105260, https://doi.org/10.1016/j.jobe.2022.105260.

[49] L.R. Gómez, N.A. García, V. Vitelli, J. Lorenzana, D.A. Vega, Phase nucleation in curved space, Nat. Commun. 6 (2015) 6856, https://doi.org/10.1038/ncomms7856.

[50] A.J. Page, R.P. Sear, Crystallization controlled by the geometry of a surface, J. Am. Chem. Soc. 131 (2009) 17550–17551, https://doi.org/10.1021/ja9085512.

[51] U. Nachshon, B. Baharier, A. Ogungbile, R. Katzir, Impact of slope inclination on salt accumulation due to bare soil evaporation, Soil Sci. Soc. Am. J. 83 (2019) 1655–1663, https://doi.org/10.2136/sssaj2019.06.0184.

[52] R. Hird, M.D. Bolton, Upward migration of sodium chloride by crystallization on non-porous surfaces, Philos. Mag. 94 (2014) 78–91, https://doi.org/10.1080/14786435.2013.843794.

[53] C15 Committee, Test Methods for Sampling and Testing Brick and Structural Clay Tile, ASTM International, West Conshohocken, PA.

[54] Y. Ge, X. Tian, D. Huang, Q. Zhong, Y. Yang, H. Peng, Understanding efflorescence behavior and compressive strength evolution of metakaolin-based geopolymer under a pore structure perspective, J. Build. Eng. 66 (2023) 105828, https://doi.org/10.1016/j.jobe.2023.105828.

[55] M. Horgnies, J.J. Chen, C. Bouillon, Overview about the use of Fourier Transform Infrared spectroscopy to study cementitious materials. Materials Characterisation VI, Siena, Italy, WIT Press, Southampton, UK, 2013, pp. 251–262.

[56] M.A. Longhi, E.D. Rodríguez, B. Walkley, D. Eckhard, Z. Zhang, J.L. Provis, A.P. Kirchheim, Metakaolin-based geopolymers: Efflorescence and its effect on microstructure and mechanical properties, Ceram. Int. 48 (2022) 2212–2229, https://doi.org/10.1016/j.ceramint.2021.09.313.

[57] A. Moropoulou, E. Zendri, P. Ortiz, E.T. Delegou, I. Ntoutsi, E. Balliana, J. Becerra, R. Ortiz, Scanning microscopy techniques as an assessment tool of materials and interventions for the protection of built cultural heritage, Scanning 2019 (2019) 5376214, https://doi.org/10.1155/2019/5376214.

[58] F. Pacheco-Torgal, J. Labrincha, C. Leonelli, A. Palomo, P. Chindaprasit (Eds.), Handbook of Alkali-Activated Cements, Mortars and Concretes, Eds., Elsevier Science, Burlington, 2014.

[59] K. Pasupathy, S. Ramakrishnan, J. Sanjayan, Effect of hydrophobic surface-modified fine aggregates on efflorescence control in geopolymer, Cem. Concr. Compos. 126 (2022) 104337, https://doi.org/10.1016/j.cemconcomp.2021.104337.

[60] R. Pernicová, Analysis of formation and testing of efflorescence on concrete elements, AMR 1025-1026 (2014) 641–644, https://doi.org/10.4028/www.scientific.net/AMR.1025-1026.641.

[61] J.P. Sanders, D.A. Brosnan, Test method for determining the efflorescence potential of masonry materials based on soluble salt content, J. ASTM Int. 7 (2010) 1–11, https://doi.org/10.1520/JAI102725.

[62] S.L. Sarkar, X. Aimin, D. Jana, Scanning Electron Microscopy, X-Ray Microanalysis of Concretes. Handbook of Analytical Techniques in Concrete Science and Technology, Elsevier, 2001, pp. 231–274.

[63] N.M. Sutan, H. Sinin, Efflorescence phenomenon on concrete structures, Adv. Mater. Res. 626 (2012) 747–750, https://doi.org/10.4028/www.scientific.net/AMR.626.747.

[64] Z. Yang, N. Xue, L. Xu, L. Yu, L. Huang, K. Wu, Evaluation of the efflorescence resistance of calcium sulfoaluminate cement mortar: from indoor accelerated testing to outdoor exposure, J. Mater. Res. Technol. 22 (2023) 2447–2461, https://doi.org/10.1016/j.jmrt.2022.12.061.

[65] A. Allahverdi, E. Najafi Kani, K. Hossain, M. Lachemi, Methods to control efflorescence in alkali-activated cement-based materials, in: F. Pacheco-Torgal, J. Labrincha, C. Leonelli, A. Palomo, P. Chindaprasit (Eds.), Eds.Handbook of Alkali-Activated Cements, Mortars and Concretes, 17, Elsevier Science, Burlington, 2014, pp. 463–483.

[66] D.V. Ribeiro, J.A.M. Agnelli, M.R. Morelli, Study of mechanical properties and durability of magnesium phosphate cement matrix containing grinding dust, Mat. Res. 16 (2013) 1113–1121, https://doi.org/10.1590/S1516-14392013005000105.

[67] J. Temuujin, A. van Riessen, R. Williams, Influence of calcium compounds on the mechanical properties of fly ash geopolymer pastes, J. Hazard. Mater. 167 (2009) 82–88, https://doi.org/10.1016/j.jhazmat.2008.12.121.

[68] L. Xu, S. Liu, P. Wang, Z. Yang, Influence of mineral additives on the efflorescence of ettringite-rich systems, Mater. (Basel) 14 (2021), https://doi.org/10.3390/ma14185464.

[69] V. Pungercar, M. Hutz, F. Musso, 3D Print with Salt, Digital Innovations in Architecture, Engineering and Construction, Springer, Cham, 2023.

[70] H. Schmeisky, O. Lenz, Zur Begrünung von Rückstandshalden der Kaliindustrie - Ergebnisse einer 25 jährigen Forschungsarbeit 134, 1998.

[71] A. Colas, Le sel, France, 1985.

[72] T. Ficker, D. Martišek, H.M. Jennings, Roughness of fracture surfaces and compressive strength of hydrated cement pastes, Cem. Concr. Res. 40 (2010) 947–955, https://doi.org/10.1016/j.cemconres.2010.02.002.

[73] J.-M. Becker, S. Grousson, M. Jourlin, Surface state analysis by means of confocal microscopy, Cem. Concr. Compos. 23 (2001) 255–259, https://doi.org/10.1016/S0958-9465(00)00081-0.

[74] K.L. Apedo, P. Montgomery, N. Serres, C. Fond, F. Feugeas, Geometrical roughness analysis of cement paste surfaces using coherence scanning interferometry and confocal microscopy, Mater. Charact. 118 (2016) 212–224, https://doi.org/10.1016/j.matchar.2016.05.023.

[75] B.L. Drake, B.L. MacDonald, W.Y. Lee, Qualitative Analysis Using pXRF 51–80. https://doi.org/10.1039/9781839162695-00051.

[76] J. Chen, J. Jia, M. Zhu, Role of supplementary cementitious materials on chloride binding behaviors and corrosion resistance in marine environment, Constr. Build. Mater. 458 (2025) 139724, https://doi.org/10.1016/j.conbuildmat.2024.139724.

[77] H. He, H. Qiao, T. Sun, H. Yang, C. He, Research progress in mechanisms, influence factors and improvement routes of chloride binding for cement composites, J. Build. Eng. 86 (2024) 108978, https://doi.org/10.1016/j.jobe.2024.108978.

[78] P. Kryvenko, P. Sikora, I. Rudenko, O. Konstantynovskyi, Advances in using seawater in slag-containing cement systems, J. Build. Eng. 96 (2024) 110386, https://doi.org/10.1016/j.jobe.2024.110386.

[79] A.A. Hanhan, Influence of the SO3 Content of Cement on the Durability and Strength of Concrete Exposed to Sodium Sulfate Environment. USF Tampa Graduate Theses and Dissertations. (2004).

[80] K.M. Alexander, J. Wardlaw, I. Ivanusec, The influence of SO3 content of portland cement on the creep and other physical properties of concrete, Cem. Concr. Res. 9 (1979) 451–459, https://doi.org/10.1016/0008-8846(79)90042-5.

[81] S. Horkoss, R. Lteif, T. Rizk, Influence of the clinker SO3 on the cement characteristics, Cem. Concr. Res. 41 (2011) 913–919, https://doi.org/10.1016/j.cemconres.2011.04.015.

[82] L. Jin, T. Wu, P. Liu, Z. Wang, P. Zhou, Macro-meso degradation evolution of fully recycled coarse aggregate concrete under sulfate attack in marine environment, Structures 69 (2024) 107536, https://doi.org/10.1016/j.istruc.2024.107536.

[83] G. Zhao, Y. Hu, S. Li, Z. Wang, M. Guo, F. Han, H. Wang, Degradation mechanisms of chloride contaminated cast-in-situ concrete partially exposed to magnesium-sulfate combined environment, KSCE J. Civ. Eng. 27 (2023) 618–629, https://doi.org/10.1007/s12205-022-0106-5.

[84] C. Rodriguez-Navarro, E. Doehne, Salt weathering: influence of evaporation rate, supersaturation and crystallization pattern, Earth Surf. Process. Landf. 24 (1999) 191–209.

[85] J.D. Smith, C. Garcia, J. Rodriguez, T.W. Scharf, Quantitative estimation of closed cell porosity in low density ceramic composites using X-ray microtomography, Sci. Rep. 13 (2023) 127, https://doi.org/10.1038/s41598-022-27114-w.